18TH WORLD CONFERENCE ON EARTHQUAKE ENGINEERING
WCEE2024
MILAN

MILAN, ITALY
30TH JUNE - 5TH JULY 2024

www.wcee2024.it

DESIGN AND EXPERIMENTAL CHARACTERIZATION OF PRESTRESSED LEAD DAMPERS

V. Quaglini[1], C. Pettorruso[1], E. Bruschi[1] & L. Zoccolini[1]

[1] Politecnico di Milano, Department Architecture, Built Environment and Construction Engineering ABC, Milan, Italy, virginio.quaglini@polimi.it, carlo.pettorruso@polimi.it, eleonora.bruschi@polimi.it, luca.zoccolini@polimi.it

Abstract: *A modern approach to improve the seismic performance of both new and existing structures is to provide the structural frame with a set of dampers where the dissipation of most of the energy input is concentrated. One of the limits of this solution is that current dampers can get damaged after a strong earthquake, leaving the structure exposed to possible aftershocks. The aim of the study is to introduce a new damper suitable to resist to multiple earthquakes that can be used in bracing systems of frame structures. The damper provides energy dissipation by the friction force that is activated between a moving shaft and a lead core prestressed within a steel chamber. Thanks to the ability of lead to restore its properties by strain relief due to static recrystallization taking place immediately after deformation, repeated cycles of loading do not produce damages, and the device can quickly recover its original performance after an earthquake. In the first part of the contribution, the conceptual design of the new damper is presented. Finite element analyses are used to predict the basic behaviour of the device and to express the dependency of the force-displacement curve from the prestress of the lead core. In the second part of the study, two prototypes of the damper are experimentally characterized by means of cyclic and ramp tests performed at different speeds and stroke amplitudes. The dampers are shown to provide a stable and repeatable response over repeated cycles, an essentially rectangular hysteresis loop with an equivalent viscous damping ratio $\xi_{eff} > 55\%$, a low sensitivity on the loading rate, and can withstand multiple cycles of deformation to the seismic design displacement without deterioration of performance, ensuring maintenance-free operation in presence of repeated ground shakes.*

1. Introduction

Strong earthquakes impose significant seismic input energy into the structures. The conventional earthquake-resistant design practice is implicitly based on the concept that most of this energy is dissipated by the structure by forming plastic hinge zones (CEN 2004; FEMA 2022). However, due to plastic deformations the structural members experience damage at different levels, i.e., concrete cracking and reinforcement yield, depending on the inelastic cyclic effects of ground motions. Therefore, the dissipation of the seismic energy is pursued by accepting some damage to the structure. On the other hand, modern earthquake-resistant design aims at avoiding structural damage by mitigating the effects of earthquakes. This effect can be achieved either by minimizing the seismic energy input, i.e., by isolating the structure from the ground, or by concentrating energy dissipation into some fuse members which are not part of the gravity-resistant frame (Christopolous and Filiatrault 2006). As the damage is concentrated in the fuse members, which can be easily replaced after an earthquake, structural members may suffer little or no damage.

Supplemental energy dissipation has indeed proven in the last years to be a viable solution for improving the seismic performance of structures, reducing acceleration, inter-story drift and shear force demand from the ground motion (Di Cesare et al. 2014; Di Cesare and Ponzo 2017, Mazza 2015, Symans et al. 2008). Current energy dissipation devices can be classified in two main categories: fluid dampers and hysteretic dampers (Christopolous and Filiatrault 2006). Fluid dampers dissipate energy through the lamination of a viscous fluid forced to pass through an orifice or a valving system, and their response mainly depends on the fluid velocity. Hysteretic dampers, whose constitutive law mainly depends on the imposed displacement, are further divided into steel hysteretic dampers, friction dampers and metal extrusion dampers, depending on the dissipation mechanism. Steel hysteretic dampers are today the most used (Durucan and Dicleli 2010; Di Cesare and Ponzo 2017; Garivani et al. 2020; Golmoghany and Zahrai 2021; Mazza and Vulcano 2014), while friction and extrusion dampers are less popular (Aiken et al. 1992; Pall et al. 1980; Robinson and Greenbank 1975, 1976). Theoretical force–displacement curves of hysteretic dampers are illustrated in Figure 1, where F is the force, d is the displacement, F_y and d_y are the yield force and the yield displacement, and F_{bd} and d_{bd} are the force at design displacement and the design displacement, respectively; the area enclosed within the hysteresis loop corresponds to the energy dissipated by the damper in a cycle.

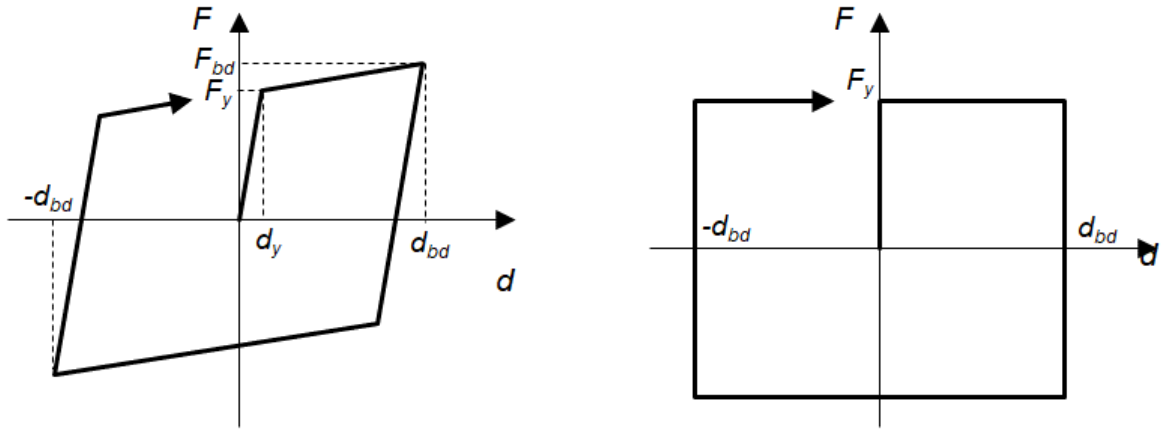

(a) (b)

Figure 1. Theoretical hysteresis loops of hysteretic dampers: (a) steel hysteretic dampers; (b), friction dampers and extrusion dampers.

The common design practice is to implement dampers into bracing systems that connect two floors, to take advantage of the interstorey drift (Christopolous and Filiatrault 2006). Though solutions for inserting the dampers into the structural frame have been the subject of many innovative suggestions, coupling to steel braces remains the most widespread approach because of its laying easiness and adaptability to any existing frame (Bartera and Giacchetti 2004, Christopoulos et al. 2008; Durucan and Dicleli 2010; Gandelli et al. 2019; Mazza and Vulcano 2014, 2015). By this design, two effects are achieved, namely increasing the structural stiffness by means of the braces, which reduces the structural displacement, and dissipating the input seismic energy, which reduces the structural acceleration (Bartera and Giacchetti 2004; Yang et al. 2021).

On the other hand, dissipative braces present some drawbacks such as the ensuing increase of internal forces in beams and columns, the modification of the building layout, and, in case of retrofit, the need of substantial construction work with heavy disturbance to the occupants, which in some situations can make their application not cost-effective (Martinez-Rueda, 2002). It has been also demonstrated that dissipative systems designed respecting the “structural safety requirement” at the Ultimate Limit State as requested by current codes (CSLLPP 2019) may be not engaged during weak ground motions, and in this case the structure provided with dampers could undergo higher accelerations than its unbraced counterpart (Gandelli et al. 2019; Ponzo et al. 2019). To overcome this issue, novel solutions to control multiple levels of earthquake energy have been proposed in the recent years (Balendra et al. 2001; Gandelli et al., 2021, Golmoghany and Zahrai 2021; Li et al. 2017; Naeem and Kim 2019). Moreover, because of low-cycle fatigue and residual stresses of steel dampers, or permanent deformation of friction and extrusion dampers, after a strong and/or long-duration earthquake hysteretic dampers need to be replaced or restated, with a cost and a potential risk for the safety

of the structure, which is left unprotected in case of aftershocks that may occur before the intervention on the dissipation system. In conclusion, a more robust form of energy dissipation system is needed that satisfies multiple goals (Rodgers et al. 2008): (i) provide a more compact and architecturally less invasive design; (ii) avoid the risk of low-cycle fatigue; (iii) do not require maintenance after a major ground motion, in order to guarantee a high safety level and provide a cost-effective solution especially for the retrofitting of ordinary buildings; (iv) ensure the re-centering of the structure, or produce a low reaction when an external re-centering action is applied; and (iv) provide a cost comparable to conventional design solutions.

A novel friction damper, called the PreStressed Lead Damper (PS-LED), has been recently proposed (Bruschi and Quaglini 2022a, 2022b, 2023; Bruschi et al. 2023; Pettorruso et al. 2021; Quaglini et al. 2021, 2022a, 2022b, 2022c) to overcome typical limitations of conventional steel hysteretic dampers. The paper illustrates the conceptual design of the PS-LED and presents the finite element analyses which were performed to predict the basic behaviour of the device, including the dependency of the force-displacement curve on the prestress of the lead core. In the second part of the paper, the experimental assessment of the PS-LED is reported, to demonstrate compliance to the requirements of the European standard EN 15129 on anti-seismic devices (CEN 2009) which is compulsory for CE Marking.

2. Conceptual design of the PS-LED

The PS-LED has a simple design, made of four main parts, which are a rigid tube, a cap, a straight shaft, and a core (Figure 2, left). Tube, shaft, and cap are made of structural steel, and the shaft is plated with hard chromium; the core is made of 99.99% pure lead. The cap is fixed to the tube by means of high strength screws. Eventually, the damper is provided with spherical joints at the opposite ends of the shaft and of the main body to avoid transmission of bending moments (Figure 2, right).

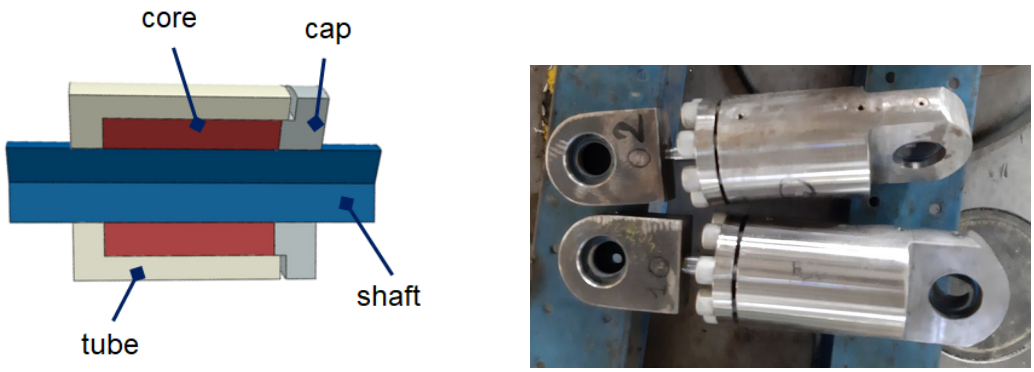

Figure 2. Longitudinal section of the PS-LED (left) and view of two prototypes (right).

The horizontal deformation of the structure in which the PS-LED is implemented triggers sliding of the shaft within the core, activating a friction force at the sliding interface by means of which energy is dissipated. As the coefficient of friction between lead and steel remains substantially steady during sliding (Pettorruso et al. 2021), the damper provides a constant force over its stroke resulting in an essentially rectangular hysteretic curve (Quaglini et al. 2022a). The theoretical amount of energy dissipated in a full cycle between d_{bd} and $-d_{bd}$ is $EDC = 4\ Fy\ d_{bd}$, where Fy and d_{bd} have been already defined.

The axial force of the damper can be expressed through the formula

$$F_y = \tau \cdot (\pi \cdot D \cdot L_c) = \mu \cdot \sigma \cdot (\pi \cdot D \cdot L_c) \qquad (1)$$

where D is the diameter of the shaft, L_c is the length of the shaft/core interface, $\tau = \mu\ \sigma$ is the shear stress e, μ is the friction coefficient and σ is the contact pressure at the shaft/core interface. Lead is chosen as core material because of its low yield strength: during assembling it can be compressed within the tube to completely fill the tube, avoiding any gaps and completely fitting the surface of the shaft. Like metals, after yielding lead behaves like an incompressible fluid; therefore, by preloading the lead core confined within the tube, it is possible to increase the contact stress at the lead/shaft interface, and consequently the force F_y (Quaglini et al. 2023a, 2023b).

The main advantages deriving by the dissipation mechanism based on friction are summarized in few points:

1. the rectangular hysteretic curve maximizes the amount of energy dissipation for a given displacement;
2. the axial force is constant regardless of the actual displacement; therefore, the PS-LED can withstand seismic inputs at different hazard levels without increasing the force transmitted to its connections or to the structure;
3. there is no component subjected to cyclic yielding during the back-and-forth motion of the shaft, avoiding low-cycle fatigue and ensuring an improved reliability during long-duration earthquakes (Bruschi and Quaglini 2022a, 2022b; Quaglini et al. 2022b);
4. the axial force of the damper can be controlled by pre-stressing the lead core within the tube, allowing to achieve high specific force with compact dimensions.

3. Numerical analyses

To investigate the influence of the prestress on the axial force of the PS-LED, a numerical model of the device was created in the general-purpose software Abaqus/CAE 6.14-2 (Simulia 2017), using 4-node bilinear axisymmetric elements type C4X4 and modelling only half of the damper due to its symmetry (Figure 3(a)). The assigned material parameters are reported in Table 1. The lead was modelled as an elastic- perfectly plastic material, though a small hardening was introduced to avoid convergence issues, and a fine mesh (3.3 mm maximum element size) was used to formulate the model of the core. S450 steel properties were assigned to the shaft, tube and cap. Hard contact was introduced at the interfaces between shaft and tube and between the shaft and cap, while hard contact in the normal direction and penalty friction formulation in the shear direction were assigned at the interfaces between the lead and shaft and between the lead and tube, with friction coefficients $\mu_1 = 0.15$ and $\mu_2 = 0.30$, respectively (Quaglini et al. 2021).

Prestressing of the lead core was simulated by applying a uniform pressure on the cap. This force was increased until a fixed axial strain $\varepsilon_c = \Delta L/L_c$ of the core was achieved, where L_c is the initial length of the core and ΔL represents the change in this dimension (Quaglini et al. 2023b). At this point, the force was held constant and dynamic implicit analysis was performed by imposing a cyclic displacement history to the shaft with a displacement amplitude of 20 mm. The analyses were performed considering different values of axial strain ε_c and different diameters of the shaft, namely D_s = 20, 28 and 32.5 mm. The outer diameter of the core was kept constant and equal to 70 mm.

The results of all the analyses are summarized in Figure 3(b). The damper force F_y increases almost proportionally with ε_c until a certain threshold is reached, beyond which no further increase occurs. This force threshold is associated with the yielding of the steel components of the damper and defines the maximum stress that can be induced in the core. A further increase in the axial strain does not entail a corresponding increase in the damper force, but leads to plasticization of the cap screws and the tube.

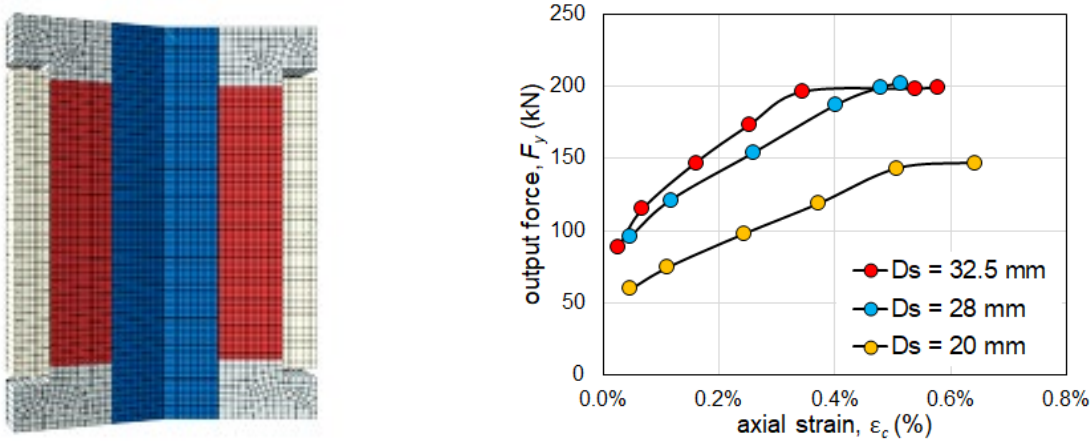

(a) (b)

Figure 3. a) finite element model of the PS-LED, adapted from Quaglini et al. (2023b); b) axial force F_y vs axial strain ε_c of lead core for different shaft diameter D_s.

Table 1. Material properties of the FE model in Abaqus.

Property	**Unit**	**Steel**		**Lead**	
Young's modulus (E)	GPa	210		16.4	
Poisson's ratio (v)	–	0.33		0.44	
Density (ρ)	kg/mm^3	7.85×10^{-6}		8×10^{-6}	
Plastic behaviour		plastic strain (m/m)	stress (MPa)	plastic strain (m/m)	stress (MPa)
		0	450	0	20.5
		0.2	500	0.001	21.5
				0.002	22.0
				0.1	22.5
				0.3	23.0

4. Prototype tests

Two prototypes of the PS-LED were manufactured with dimensions shown in Table 2. Here D_s is the shaft diameter, D_c is the outer diameter of the core, L_c is the length of the core (corresponding to the length of the shaft/core interface), and L_s is the total length of the shaft. The first prototype (PS-LED 220-10) is designed for a seismic displacement d_{bd} = 10 mm and an axial force F_y = 220 kN, while the second prototype (PS-LED 50-15) is designed for d_{bd} = 15 mm and F_y = 50 kN.

Table 2. Dimensions of PS-LED prototypes.

ID	**D_s (mm)**	**D_c (mm)**	**L_s (mm)**	**L_c (mm)**
PS-LED 220-10	32.5	60	410	80
PS-LED 50-15	20	70	385	70

The two prototypes were subjected to the experimental protocol shown in Table 3, where d_o is the displacement amplitude, or the maximum displacement imposed in the test, f_o is the testing frequency, and N is the number of cycles. The tests were performed at the Materials Testing Laboratory of Politecnico di Milano, using a 500 kN servohydraulic testing machine (MTS Systems, Eden Prairie, MN), Figure 4. Four types of tests were performed on each prototype, namely the cyclic test (CT), the ramp test (RT), the dynamic test (DT) and the repeated loading test (RLT). The cyclic test and the ramp test are prescribed by the European Standard EN 15129 (CEN 2009) for Displacement Dependent Devices (DDD). In the cyclic test, sinusoidal cycles of increasing amplitude at 25%, 50% and 100% of the design displacement d_{bd} were imposed to the test specimen, performing five cycles at the lowest and intermediate amplitudes, and ten cycles at the maximum amplitude. The loading frequency was f_0 = 0.5 Hz for prototype PS-LED 220-10, and 0.25 Hz for prototype PS-LED 50-15. In the ramp test a monotonic ramp at 0.1 mm/s was imposed up the amplified displacement $\gamma_b \gamma_x d_{bd}$ where γ_b = 1.1 is the amplification factor and γ_x = 1.2 is the reliability factor. To be conservative, the ramp test was performed considering two times the amplified displacement recommended in the standard (CEN 2009).

The effect of speed on the response of the PS-LED was investigated through dynamic tests, where the test specimen was subjected to five sinusoidal cycles with constant amplitude d_{bd} and different frequencies, performing 4 cycles at each frequency.

Finally, the repeated loading test was conducted. Three sequences of ten cycles each with amplitude equal to d_{bd} were imposed to the prototypes, with a dwell period of about 1 hour between two consecutive sequences.

Table 3. Dimensions of PS-LED prototypes, adapted from (Quaglini et al. 2023a).

Test	d_o (mm)	f_o (Hz)	N (#)
cyclic	0.25 d_{bd}	f_0	5
	0.5 d_{bd}	f_0	5
	1.0 d_{bd}	f_0	10
ramp	$2 \cdot \gamma_x \cdot \gamma_b \cdot d_{bd}$	0.001	1
dynamic	1.0 d_{bd}	0.5 f_0	4
	1.0 d_{bd}	1.0 f_0	4
	1.0 d_{bd}	1.5 f_0	5
repeated loading	1.0 d_{bd}	f_0	10
	1.0 d_{bd}	f_0	10
	1.0 d_{bd}	f_0	10

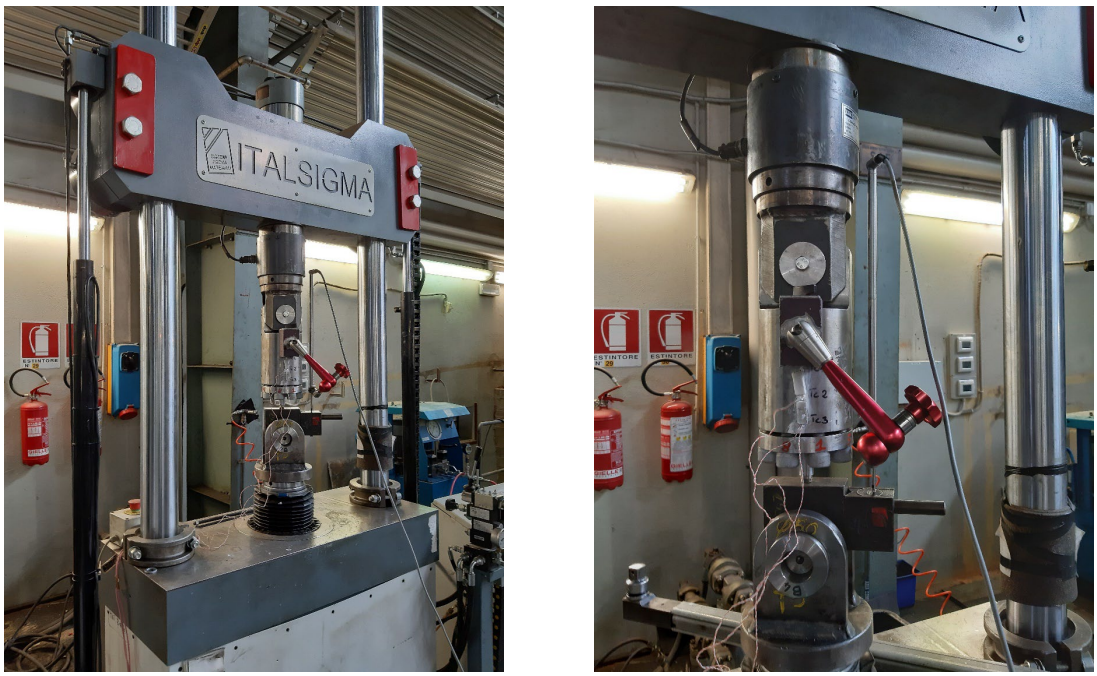

Figure 4. Test specimen installed on the testing frame (left) and close-up view (right), with details of connections at the spherical hinges and the external displacement transducer.

The experimental force–displacement hysteresis loops of the two PS-LED prototypes are shown in Figure 5. The plots show an elastic branch, which corresponds to the elastic deflection of the shaft before sliding of the shaft is triggered, followed by a plastic branch with a constant force regardless of the displacement; the yield force is the same both in extension ($F > 0$, shaft moving outwards) and in compression ($F < 0$, shaft moving inwards). The hysteresis loop shows a small curvature at each motion reversal, which may denote a shallow dependence of the friction force on the velocity, though this dependency does not affect too much the overall response. The idle displacement observed after the motion reversal is an effect of the clearance of the spherical hinges at the two ends of the damper.

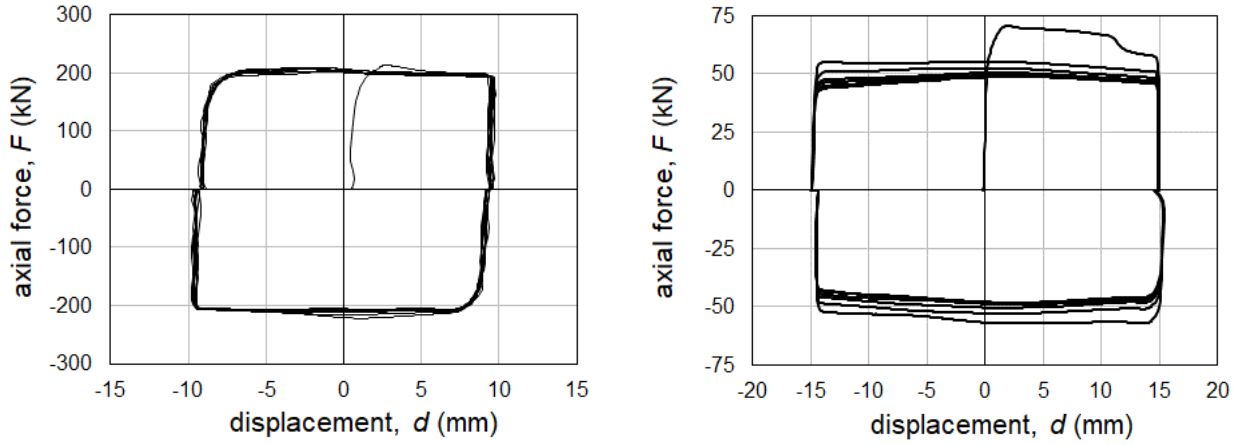

Figure 5. Experimental force–displacement loops: (a) PS-LED 220-10; (b) PS-LED 50-15.

The response of the PS-LED is evaluated based on effective stiffness K_{eff} and the equivalent viscous damping ratio ξ_{eff}, which are determined through the formulas

$$K_{eff} = \frac{F_{d_o}}{d_o} \tag{2}$$

$$\xi_{eff} = \frac{2\,EDC}{\pi\, d_o\, F_{d_o}} \tag{3}$$

where d_o is the maximum displacement in a cycle, F_{do} is the force at d_o , and *EDC* is the energy dissipated per cycle.

The consistent behaviour of the PS-LED during repeated cycles was evaluated in the cyclic test. Disregarding the first cycle, both K_{eff} and ξ_{eff} remain stable over each sequence of cycles (Figure 6), with a variation less than 10% with respect to the relevant values evaluated at the third cycle of the sequence, fulfilling the requirements for Displacement Dependent Devices prescribed in the European standard EN 15129 (CEN 2009). In particular, in the most challenging sequence of cycles to the design displacement d_{bd}, the maximum variations on K_{eff} and ξ_{eff} were of 3.4% and 1.7% for PS-LED 220-10, and of 7.6% and 0.9% for PS-LED 50-15, respectively. The average value of ξ_{eff} over 10 cycles performed at d_{bd} is ξ_{eff} = 0.55 for PS-LED 220-10 and ξ_{eff} = 0.60 for PS-LED 50-15, very close to the maximum theoretical value of 0.63. Only during the tests on PS-LED 220-10 at 0.25 d_o, ξ_{eff} was about 0.40; this was attributed to the experimental bias introduced by the plays of the test set-up, and in particular of the spherical joints of the damper, which were not negligible in comparison to the displacement amplitude (i.e., 2.5 mm). It is worth to recall that for standard buckling-restrained steel hysteretic dampers, the equivalent viscous damping ratio ξ_{eff} typically lies in the range of 0.20 to 0.40, depending on the geometry and the design deflection (Sina et al. 2021; Sitler et al. 2020; Tonon et al. 2013).

In the ramp test the prototypes were able to sustain the amplified design deflection $2 \cdot \gamma_x \cdot \gamma_b \cdot d_{bd}$ without cracking; moreover, the force–deformation curves were monotonically increasing up to $\cdot \gamma_x \cdot \gamma_b \cdot d_{bd}$ (Figure 7), demonstrating the ability of the PS-LED to withstand, with increased reliability, the design displacement without suffering of any deterioration in stiffness.

Eventually, the two prototypes were subjected to three sequences of 10 cycles each at the design displacement d_{bd}, performed within a short time (about 1 hour of dwelling between two sequences). Prestressing was applied to the lead core only before the first sequence; similarly, the device was not recentered after each sequency. The mechanical response of the damper was stable and predictable, showing no substantial change in stiffness or damping throughout the three sequences (Figure 8).

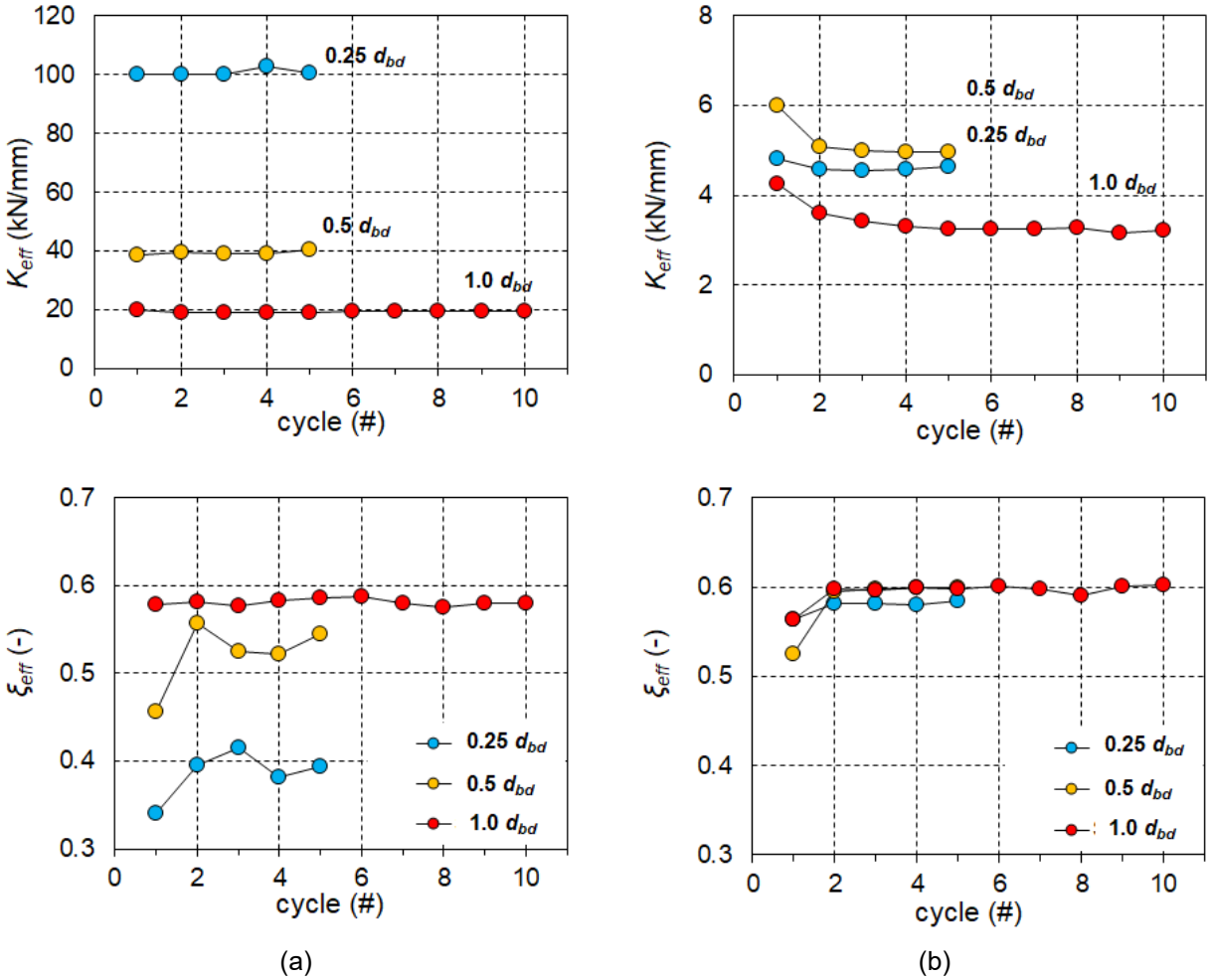

Figure 6. Effective stiffness K_{eff} and equivalent viscous damping ξ_{eff} vs. number of cycles at different amplitudes d_o: (a) PS-LED 220-10; (b) PS-LED 50-15.

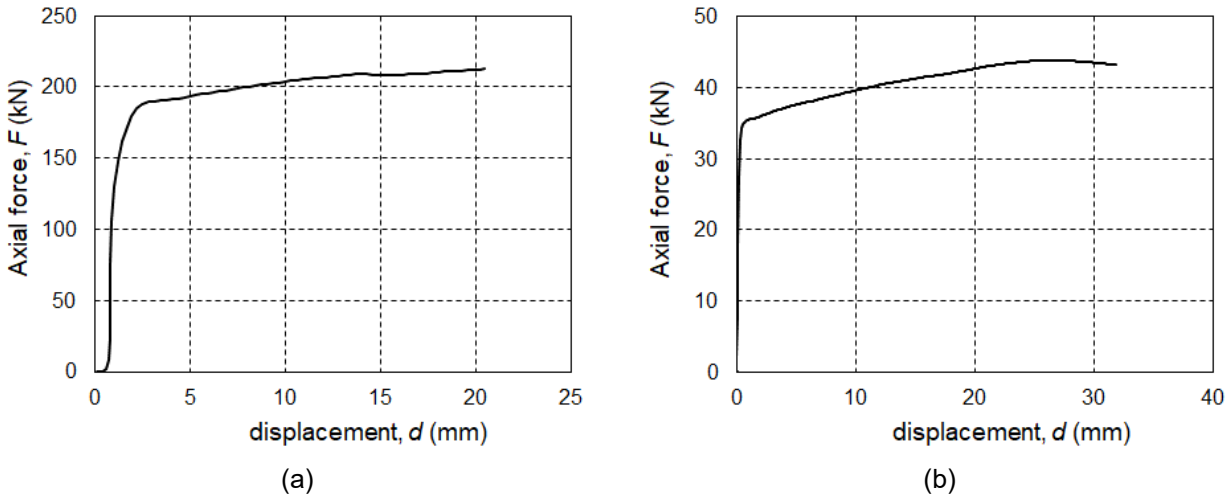

Figure 7. Ramp test to the amplified design deflection $2 \cdot \gamma_x \cdot \gamma_b \cdot d_{bd}$: (a) PS-LED 220-10; (b) PS-LED 50-15.

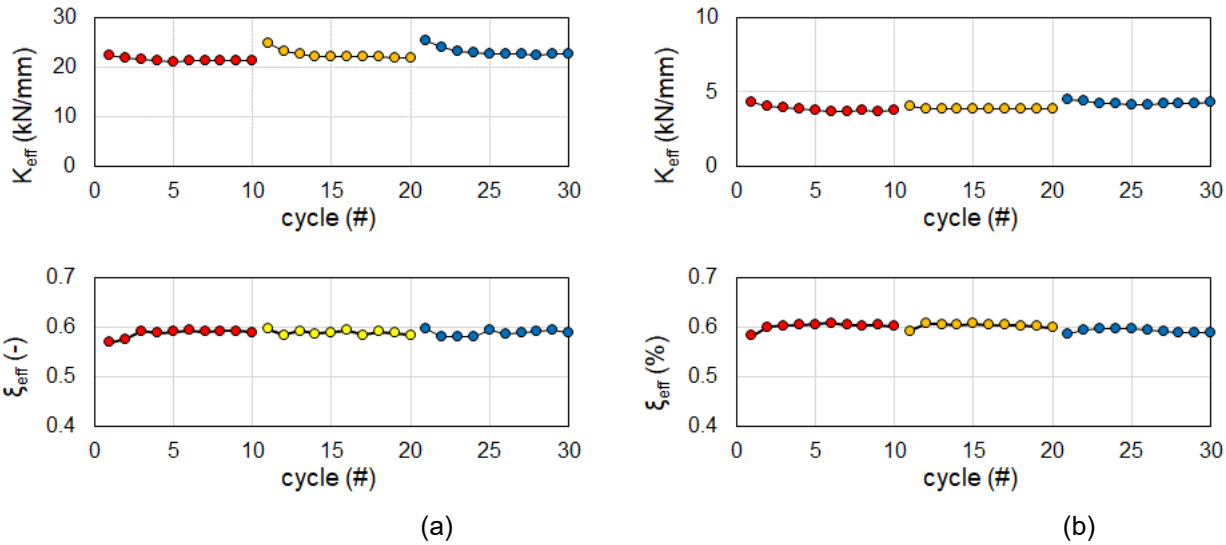

Figure 8. Effective stiffness K_{eff} and equivalent viscous damping ξ_{eff} vs. number of cycles evaluated over three sequences at d_{bd}: (a) PS-LED 220-10; (b) PS-LED 50-15.

5. Conclusions

In this paper the design and the experimental evaluation of the Prestressed Lead Damper, or PS-LED, have been presented. The tests were performed on two devices with different force and displacement capacities. The main results are summarized hereinafter:

1. the PS-LED is characterized by an essentially rigid–plastic hysteresis loop, with a constant output force independent of the displacement; at the design displacement the equivalent viscous damping ratio was between 0.55 and 0.60;
2. the axial force of the PS-LED can be controlled by prestressing the lead core during assembling;
3. the two prototypes showed a consistent mechanical behaviour over ten cycles at the design seismic displacement, fulfilling the limits of variation prescribed in the European standard (CEN 2009);
4. the prototypes were able to withstand multiple sequences of motion at the design seismic displacement, demonstrating the ability to provide maintenance-free operation even in presence of repeated ground shakes.

In conclusion, thanks to the ability to withstand several design level strong motions without needing maintenance, and its high damping capability coupled to a compact design, the PS-LED is potentially suitable to overcome the main limits that affect current supplementary energy dissipation devices.

6. Acknowledgements

This research was partially funded by the Department of the Italian Civil Protection (DPC) in the Frame of the National Research Project DPC – ReLUIS (National Network of Laboratories of Seismic Engineering) 2019–2021, Work Package 15 “Regulatory Contributions for Isolation and Dissipation”.

7. References

Aiken I.D., Nims D.K., Kelly J.M. (1992). Comparative study of four passive energy dissipation systems, *Bulletin of New Zealand National Society of Earthquake Engineering*, 25(3): 175–192.

Balendra T., Yu C.H., Lee F.L. (2001). An economical structural system for wind and earthquake loads, *Engineering Structures*, 23: 491–501.

Bartera F., Giacchetti R. (2004). Steel dissipating braces for upgrading existing building frames, *Journal of Constructional Steel Research*, 60: 751-769.

Bruschi E., Quaglini V. (2022a). Assessment of a novel hysteretic friction damper for the seismic retrofit of reinforced concrete frame structures, *Structures*, 46: 793-811.

Bruschi E., Quaglini V. (2022b) Modelling of a novel lead damper and application to an existing RC structure, *Lecture Notes in Civil Engineering*, 326 LNCE: 52-62.

Bruschi E., Quaglini V. (2023) Numerical investigation on the seismic performance of a RC framed building equipped with a novel Prestressed LEad Damper with Straight Shaft, *Structural Integrity Procedia*, 44(C): 1443-1450.

Bruschi E., Zoccolini L., Cattaneo S., Quaglini V. (2023). Experimental characterization, modelling and numerical evaluation of a novel friction damper for the seismic upgrade of existing buildings, *Materials*, 16(5): paper 1933.

CEN (2004). *EN 1998-1:2004: Eurocode 8: Design of structures for earthquake resistance – Part 1: General rules, seismic actions and rules for buildings*, Comité Européen de Normalisation, Brussels.

CEN (2009). *EN 15129:2009. Anti-seismic devices*, Comité Européen de Normalisation, Brussels.

Christopolous C., Filiatrault A. (2006). *Principles of passive supplemental damping and seismic isolation*, Pavia: IUSS Press.

Christopolous C., Tremblay R., Kim H.-J., Lacerte M. (2008). Self-centering energy dissipative bracing system for the seismic resistance of structures: development and validation, *ASCE Journal of Structural Engineering*, 134(1): 96-107.

CSLLPP (2019). *Circolare 21 gennaio 2019, n. 7 C.S.LL.PP. Istruzioni per l'applicazione dell'«Aggiornamento delle "Norme tecniche per le costruzioni"» di cui al decreto ministeriale 17 gennaio 2018*, Rome: Public Works Council (in Italian).

Di Cesare A., Ponzo F.C., Nigro D. (2014). Assessment of the performance of hysteretic energy dissipation bracing systems, *Bulletin of Earthquake Engineering*, 12(6): 2777–2796.

Di Cesare A., Ponzo F.C. (2017). Seismic retrofit of reinforced concrete frame buildings with hysteretic bracing systems: design procedure and behaviour factor, *Shock and Vibration*, 2017: Article ID 2639361.

Durucan C., Dicleli M. (2010). Analytical study on seismic retrofitting of reinforced concrete buildings using steel braces with shear link, *Engineering Structures*, 32: 2995-3010.

FEMA (2022). *FEMA P-749:2022, Earthquake-resistant design concepts: an introduction to seismic provisions for new buildings*, Washington DC: Federal Emergency Management Agency.

Gandelli E., Taras A., Distl J., Quaglini V. (2019). Seismic retrofit of hospitals by means of hysteretic braces: influence on acceleration-sensitive non-structural components, *Frontiers in Built Environment*, 5: Article 100.

Gandelli E., Chernyshov S., Distl J., Dubini P., Weberd F., Taras A. (2021). Novel adaptive hysteretic damper for enhanced seismic protection of braced buildings, *Soil Dynamics and Earthquake Engineering*, 141: Article 106522.

Garivani S., Askariani S.S., Aghakouchak A.A. (2020). Seismic design of structures with yielding dampers based on drift demand, *Structures*, 28: 1885-1899.

Golmoghany M.Z., Zahrai S.M. (2021). Improving seismic behavior using a hybrid control system of friction damper and vertical shear panel in series, *Structures*, 31: 3693-79.

Li Z., Dong H., Wang X., He M. (2017). Experimental and numerical investigations into seismic performance of timber-steel hybrid structure with supplemental dampers, *Engineering Structures*, 151: 33-43.

Martínez-Rueda J.E. (2002). On the evolution of energy dissipation devices for seismic design, *Earthquake Spectra*, 18(2): 309-346.

Mazza F. (2015) Comparative study of the seismic response of RC framed buildings retrofitted using modern techniques, *Earthquakes and Structures*, 9(1): 29-48.

Mazza F., Vulcano A. (2014). Equivalent viscous damping for displacement-based seismic design of hysteretic damped braces for retrofitting framed buildings, *Bulletin of Earthquake Engineering*, 12: 2797-2819.

Mazza F., Vulcano A. (2015). Displacement-based design procedure of damped braces for the seismic retrofitting of r.c. framed buildings, *Bulletin of Earthquake Engineering*, 13: 2121-2143.

Naeem A., Kim J. (2019). Seismic performance evaluation of a multi-slit damper, *Engineering Structures*, 189: 332-346.

Pall A.S., Marsh C., Fazio P. (1980). Friction Joints for Seismic Control of Large Panel Structures, *Journal of Prestressed Concrete Institute*, 25 (6): 38-61.

Pettorruso C., Bruschi E., Quaglini V. (2021). Supplemental energy dissipation with pre-stressed Lead Extrusion Dampers (P-LED): experiments and modeling. *Proceedings of the 8th ECCOMAS Thematic Conference on Computational Methods in Structural Dynamics and Earthquake Engineering*, Athens, Greece.

Ponzo F.C., Di Cesare A., Lamarucciola N., Nigro D. (2019). Seismic design and testing of post-tensioned timber buildings with dissipative bracing systems, *Frontiers in Built Environment*, 5: Article 104.

Quaglini V., Pettorruso C., Bruschi E. (2021). Experimental and numerical assessment of pre-stressed lead extrusion dampers, *International Journal of Earthquake Engineering*, XXXVIII: 46-69.

Quaglini V., Pettorruso C., Bruschi E. (2022a). Design and experimental assessment of a pre-stressed lead damper with straight shaft for seismic protection of structures, *Geosciences*, 12: paper 182.

Quaglini V., Bruschi E., Pettorruso C. (2022b). Design and experimental characterization of a novel Lead Damper for seismic protection of buildings. *Proceedings of the 3rd European Conference on Earthquake Engineering & Seismology*, Bucharest, Romania.

Quaglini V., Bruschi E., Pettorruso C., Sartori M. (2022c). Design and experimental assessment of a novel damper with high endurance to seismic loads. *Structural Integrity Procedia*, 44(C): 1451-1457.

Quaglini V., Bruschi E., Pettorruso C., Sartori M. (2023a). Development of a novel Prestressed Lead Damper with Straight Shaft for seismic protection of structure, in: *Life-Cycle of Structures and Infrastructure Systems,* London: CRC Press.

Quaglini V., Bruschi E., Pettorruso C., Sartori M. (2023b). Design, testing and modeling of a novel friction damper with enhanced resistance to repeated seismic loads, *Proceedings of the 9th ECCOMAS Thematic Conference on Computational Methods in Structural Dynamics and Earthquake Engineering*, Athens, Greece.

Robinson W.H., Greenbank L.R. (1975). Properties of an extrusion energy absorber, *Bulletin of the New Zealand National Society for Earthquake Engineering*, 8(3): 187-191.

Robinson W.H., Greenbank L.R. L.R. (1976). An extrusion energy absorber suitable for the protection of structures during an earthquake, *Earthquake Engineering & Structural Dynamics*, 4(3): 251-259

Rodgers G.W., Mander J.B., Chase J.G., Dhakal R.P., Leach N.C., Denmead C.S. (2008). Spectral analysis and design approach for high force-to-volume extrusion damper-based structural energy dissipation, 37(2): 207-223.

Simulia (2017). *Abaqus/CAE user's guide*, Providence: Dassault Systemes Simulia Corp.

Symans M.D., Charney F.A., Whittaker A.S., Constantinou M.C., Kircher C.A., Johnson M.W., McNamara J. (2008). Energy dissipation systems for seismic applications: current practice and recent developments, *ASCE Journal of Structural Engineering*, 134(1): 3-22.

Sina F., Amir H.A., Lars D. (2021). Equivalent viscous damping for buckling-restrained braced RC frame structures, *Structures*, 34: 1229–1252.

Sitler B., Takeuchi T., Matsui R., Terashima M., Terazawa Y. (2020). Experimental investigation of a multistage buckling-restrained brace, *Engineering Structures*, 213: paper 110482.

Tonon E., Forte M., Mammino A., Moro S. (2013). Protezione sismica degli edifici mediante dissipatori d'energia: Applicazione pratica della nuova sede della prefettura de L'Aquila. *Proceedings of the XV Conference of the Italian Association of Seismic Engineering ANIDIS*, Padua, Italy.

Yang F., Wang G., Li M. (2021). Evaluation of the seismic retrofitting of mainshock-damaged reinforced concrete frame structure using steel braces with soft steel dampers, *Applied Science*, 11: Article 841.